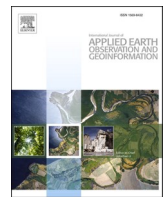


Contents lists available at ScienceDirect

International Journal of Applied Earth Observation and Geoinformation

journal homepage: www.elsevier.com/locate/jag



Quantifying heat-related risks from urban heat island effects: A global urban expansion perspective



Ming Hao ^{a,b}, Xue Liu ^{a,b,*} , Xia Li ^{a,b,*}

^a Key Lab of Geographic Information Science (Ministry of Education), School of Geographic Sciences, East China Normal University, 500 Dongchuan Rd, Shanghai 200241, China

^b Key Laboratory of Spatial-temporal Big Data Analysis and Application of Natural Resources in Megacities, Ministry of Natural Resources, Shanghai 200241, China

ARTICLE INFO

Keywords:

Urban heat island
Urban expansion
Dynamic urban boundary
Heat-related risk

ABSTRACT

Quantifying the urban heat island (UHI) effect and its impact on summer heat-related risk is important for both urban environment and human well-being. Existing studies frequently adopt the static (fixed) urban boundary to define urban/rural area in UHI measurement, overlooking the exacerbation of the urbanization-induced warming during long-term urban expansion and the consequent increase in urban heat risks. Here we measured the global surface UHI (SUHI) intensity up to 7,554 urban patches during 2000–2015 using every five-year dynamic urban boundary, followed by a two-stage analysis based on a Distributed Lag Non-linear Model (DLNM) to quantify the additional heat-related risks caused by the urbanization-induced warming. Our results show that the global average SUHI intensity increased by approximately 10 % in 15 years with distinct seasonal and diurnal variations. The global urban expansion from 2000 to 2015 resulted in an average increase of 0.61 °C (95 % CI = 0.56 °C–0.66 °C) in summer UHI intensity for newly built-up areas. This urbanization-induced warming further leads to a 20 % (95 % CI = 14.8 %–25.2 %) increase in summer heat relative risk (RR) on average, which implied an average increase of 20 % (95 % CI = 14.8 %–25.2 %) in annual heat-related mortality for the newly built-up areas. Furthermore, over 2.3 % of the world population would experience an RR increase greater than 10 %. This study highlights the importance of dynamic urban boundary for long-time span UHI measurements, providing a deeper understanding of the role of urbanization-induced warming on urban heat risk.

1. Introduction

In the past few decades, the world has experienced a rapid and sustained process of urbanization (Elmqvist et al. 2013), resulting in urban heat island (UHI) effect, which has brought negative impacts on human health from multiple perspectives such as urban air quality and summer extreme heat risks (Phelan et al. 2015). UHI effect is a phenomenon that the temperature in urban areas is significantly higher than the surrounding suburbs (Oke 2002). Existing studies usually use the temperature difference between the built-up area of a city and its surrounding natural environment (such as vegetation and bare land) to measure UHI intensity (Zhou et al. 2016). At present, most cities with a population over one million in the world are accompanied by strong UHI intensity, such as Shanghai (7 °C) (Tran et al. 2006), New York (5.4 °C) (Gaffin et al. 2008), London (8.4 °C) (Kolokotroni and Giridharan 2008), Delhi (8.3 °C) (Mohan et al. 2013), and Sydney (4 °C) (Sharifi and Lehmann 2014). Studies have shown that the UHI intensity of large

cities with dense buildings (e.g. Tokyo) even exceeded 12 °C (Tran et al. 2006). The warming effect brought by the UHI leads to an increasing vulnerability of urban residents, accounting for more than half of the world's population, to the risk of extreme high temperature (Huang et al. 2019), resulting in an increase in heat-related mortality. With the urban expansion, more urban population will be affected by stronger UHI effect in the future (Zhu et al. 2021). Therefore, exploring the impact of urban expansion on the UHI effect and its subsequent influence on urban heat risk is of significant importance.

Various methods and datasets have been developed to estimate the UHI intensity at multi-scales, such as the country scale (Imhoff et al. 2010), the continental scale (Tran et al. 2006; Zhou et al. 2013), and the global scale (Chakraborty and Lee 2019). These studies involved different study periods, from one year (Clinton and Gong 2013) to decades (Stone, 2007), and also different ways to measure UHI effect, which can be divided into atmospheric urban heat island (AUHI) effect obtained from meteorological station data (Arnfield 2003; Stewart

* Corresponding authors at: School of Geographic Sciences, East China Normal University, 500 Dongchuan Road, Shanghai 200241, China.

E-mail addresses: liuxue@geo.ecnu.edu.cn (X. Liu), lixia@geo.ecnu.edu.cn (X. Li).

2011) and surface urban heat island (SUHI) effects obtained from the thermal bands of satellite images (Voogt and Oke 2003). Moreover, these studies also investigated the spatial distribution of UHI (Clinton and Gong 2013), and its diurnal pattern (Peng et al. 2012) and seasonal variation (Shastri et al. 2017), as well as its relationship with urban size (Zhou et al. 2013), urban form (Zhou et al. 2017) and climate (Zhao et al. 2014).

For SUHI intensity, it is measured by calculating the difference of surface temperature between urban/built-up and non-urban/rural areas (Voogt 2007). The accurate measurement by the above methods relies on a precise urban/rural delineation. In rapidly urbanizing area, urban/rural boundary is constantly changing due to urban expansion (Liao et al. 2018). For global-scale SUHI studies, it is often more difficult to continuously update the urban boundary of these regions (Yao et al. 2018). As a result, many studies tend to adopt static urban boundary based on land use data from a specific baseline year and keeping them constant in subsequent years (Kim and Brown 2021). For instance, Chakraborty and Lee (2019) measured global SUHI intensity from 2000 to 2017 while keeping the urban boundary fixed at the year 2001. Similarly, the widely used Global Urban Heat Island Data Set (CIESIN - Columbia University 2016) calculated the SUHI intensity for global cities in 2013 using urban boundary from 1995. However, over a longer time span, urban boundary in rapidly urbanizing areas continue to expand due to urban growth. If the SUHI intensity is estimated based on the original static urban-rural boundary, the results will significantly deviate from reality (Liao et al. 2017). Besides, the SUHI effect of the newly built-up areas formed by urban expansion is completely neglected.

Comparing to urban static boundary, dynamic urban boundary considering urban expansion can more accurately reflect the dynamic changes in urban/rural boundary and measure long-term SUHI (Si et al. 2022). Some studies have attempted to measure long-term SUHI intensity by adopting dynamic urban boundary at various scales, e.g., global, regional, and local (Liu et al. 2022b; Si et al. 2022; Wang et al. 2020). However, a lot of the most recent studies continue to employ static urban boundary (Li et al. 2023; Zhou et al. 2023), indicating that using static boundary are still the mainstream in long-term SUHI measurements. But in this static boundary framework, the impact of urban expansion on SUHI in newly built-up areas is ignored.

Additionally, as urban continue to expand, urban population is increasing and have exceed 50 % of the total population (United Nations, 2019). SUHI can have a negative impact on the health of urban residents (Zhang et al. 2023). Many studies have shown that urbanization-induced warming in urban areas increases the risk of urban residents being exposed to extreme heat during summer, leading to a rise in heat-related mortality (Abrar et al. 2022; Pappalardo et al. 2023). The process of long-term urban expansion transforms natural vegetation around cities into impervious surfaces, contributes to the SUHI effects of these newly built-up areas (Si et al. 2022), further increasing their summer heat-related risks. Consequently, urban expansion has a potential impact on the urban heat-related risks by affecting SUHI. Although there have been many relevant studies about the urban heat risk from SUHI effect (Fu et al. 2022; Ho et al. 2023; Zhu and Yuan 2023). These studies often focus on large cities that already exhibit significant SUHI effects, such as Beijing and Chongqing (Liu et al. 2022a; Liu et al. 2020). However, the urban expansion processes in these large cities have often slowed or ceased (United Nations, 2019). In contrast, the SUHI effects and their impacts on urban heat risks in newly built-up areas formed during urbanization have been overlooked. Therefore, to understand the effects of urban expansion on urban heat risks, it is essential to focus on newly built-up areas. However, in the current state of research, studies specifically focused on the heat risk caused by intensified urbanization-induced warming remains scarce and the risk has not been quantified at global scale. With the continuous influx of urban populations (Li et al. 2022), the increasing heat-related risks arising from the intensified SUHI effects in these newly built-up areas

warrant greater attention.

To address above limitations, this study investigated the SUHI intensity of global cities in 2000/2005/2010/2015 by using dynamic urban boundary updated every 5 years, covering a long-time span and over 7,500 urban patches of different sizes and climatic zones worldwide. Then, based on dynamic urban boundary, this study identified SUHI intensity of newly built-up urban areas formed during urban expansion from 2000 to 2015. Furthermore, we converted the SUHI intensity into AUHI intensity and calculated the increase in summer heat-related risks due to the urbanization-induced warming in these areas, thereby quantifying the impact of global urban expansion on human exposure to summer heat risks. We aim to address the following three scientific questions: 1) What is the dynamic evolution of SUHI intensity in global cities under urban expansion? 2) Did the newly built-up areas have significant urbanization-induced warming? 3) How to quantify the increased urban heat risk resulting from urban expansion?

2. Data and methods

2.1. Global datasets

The primary datasets used in this study include: Global Urban Boundary (GUB) dataset, which provides dynamic delineation of urban/rural boundary for global cities (Li et al. 2020); the MODIS global surface temperature data, utilized to calculate SUHI intensity and we selected MOD11A2.v6 Terra surface temperature data for its longer temporal coverage (Wan et al., 2015). Besides, MODIS water mask (Carroll et al., 2017) ensured that we excluded water body factors from the SUHI measurement process. The GHCN-d (v3) meteorological station data (Menne et al. 2012) was employed to collect local air temperature data and establish a conversion relationship between surface temperature and air temperature. Mortality data from the Short-term Mortality Fluctuations (STMF) for countries in Europe, Asia, and Australia (Jdanov et al. 2021) and weekly mortality data provided by the U.S. Centers for Disease Control and Prevention (CDC) for U.S. states (Centers for Disease Control and Prevention 2018–2021), along with ERA5 historical climate dataset (Hersbach et al. 2020), were used to establish exposure-response curves for temperature and relative risk. The WorldPop 2015 global population data (Lloyd et al. 2019) were employed to assess the population affected by increased heat risk (Table 1).

2.2. Quantifying SUHI intensity under urban dynamic boundary

It is expected that urban dynamic will have severe influences on quantifying SUHI effect accurately. The solution is to calculate temperature differences with a more immediate, accurate urban-rural delineation scheme. Therefore, we first calculated the changes in SUHI

Table 1
Data sources of the study.

Name	Time	Resolution	Source
GUB urban boundary	2000–2015, 5-year interval	Shapefile	Li et al. 2020
MOD11A2.v6 Surface Temperature	2000–2015, 8-day average	1-km	Wan 2015
MODIS water mask	2000	250-m	Carroll 2017
GHCN-d (v3) air temperature records	2000–2015, daily	/	Menne et al. 2012
STMF mortality records	2000–2017 weekly	/	Jdanov et al. 2021
Weekly mortality records (US. CDC)	2017–2018 weekly	/	wonder.cdc.gov
ERA5 historical climate	2000–2018 daily	0.1°	Hersbach et al. 2020
WorldPop population grids	2015	1-km	Lloyd et al. 2019

in newly built-up areas that underwent urban expansion from 2000 to 2015 based on dynamic urban boundary and then converted the SUHI intensity into AUHI intensity. Next, we conducted a two-stage analysis based on a Distributed Lag Non-linear Model (DLNM) to derive changes in relative risk from the changes in AUHI intensity. Finally, we overlapped the RR results with spatial population data to quantify the population affected by the increased urban heat risk. The process of the methodology used in this study is illustrated in Fig. 1.

We calculated the SUHI intensity according to the following equation (Clinton and Gong 2013; Zhou et al. 2017; Zhou et al. 2013):

$$\Delta T = T_{\text{urbanPatch}} - T_{\text{ruralPatch}} \quad (1)$$

where ΔT is the SUHI intensity, $T_{\text{urbanPatch}}$ is the urban average surface temperature, and $T_{\text{ruralPatch}}$ represents the rural average surface temperature.

To separate urban and their surrounding rural boundary dynamically, we first extracted every five-year global urban patches from GUB product produced by Li et al. (2020) from 2000 to 2015. We followed the method of Zhang et al. (2004) to exclude all the urban patches less than 10 km² so that those small cities with insignificant SUHI or temperature data difficult to cover accurately will not be counted for the measurement. In 2000, 2005, 2010 and 2015, the number of cities worldwide for SUHI intensity measurement was 5,643, 6,456, 7,113 and 7,554 respectively. Then, we simplified the boundary of urban patches for further calculation. We built buffer zones of appropriate size based on these urban boundaries to serve as their peripheral rural area.

Previous studies usually adopted the percentage of urban area (usually 50 %-150 %) (Zhou et al. 2013) or unified buffer distance such as 5 km (Clinton and Gong 2013) or 10 km (Manoli et al. 2019), to control the size of the buffer zone. But for a study that include thousands of global cities of different sizes, it is very difficult to set a unified buffer distance to ensure that each city can get an appropriate buffer zone (rural area). To account for the unique urban form of each urban patch when creating buffer zone, we used the patch compactness index (Osserman 1978) to control the buffer area and ensured that the buffer size falls within 50 % to 150 % of the urban patch area.

We first established an 150 % area buffer zone for each urban patch. Then the patch compactness index with a range of [0,1] (Osserman 1978) that can characterize the urban form was used to adjust the buffer area. Patch compactness index (Osserman 1978) is a kind of patch shape

index, which is used to measure the compactness of urban patch shape:

$$PCI = \frac{4\pi u}{P^2} \quad (2)$$

where PCI is the compactness index of urban patch, u is the area of the patch, and P is the perimeter of the urban patch. If the urban form is more extensive, its PCI value is closer to 0, the more compact the urban form is, the closer its PCI value is to 1. When the urban form reaches the most compact ideal form (i.e. normal circle), its PCI is equal to 1. Consequently, the index PCI measures the compactness of the shape of the urban patch compared with the normal circle. Therefore, the PCI index can be used to modify the buffer area:

$$A = a \times PCI \quad (3)$$

where A is the modified buffer area for each urban patch, a is 150 % area buffer zone for each urban patch. Due to the PCI values ranging from 0 to 1, a PCI calculation approaching 0 for a given urban patch results in a very small buffer area. Therefore, in conjunction with prior research (Zhou et al., 2013), we replaced the buffer area for patches with an area less than 50 % of the urban patch to be 50 % of the urban patch area. Ultimately, each urban patch generates a buffer based on its unique urban form with the buffer size falling within 50 % to 150 % of the urban patch area.

After the dynamic urban/rural boundary extraction, for each city, we calculated the average surface temperature of urban/rural area respectively and the SUHI intensity (the temperature difference between urban/rural). The temperature data were processed as follows: 1) according to the information provided by the quality control (QC) band of Terra products, the temperature pixels with error value greater than 2°C were eliminated in this study; 2) In order to eliminate the impact of water bodies (especially inland water bodies) on the temperature calculation, the temperature pixels located in the water body area were masked according to the global water body mask, so that they did not participate in the calculation of average temperature; and 3) the pixels retained after the above process were valid pixels used to calculate the average surface temperature. In addition, we set that only when the area of valid pixels accounts for more than half of the urban/rural area, the temperature calculation results in this city will be accepted, in case that the valid pixels only account for a small part of urban/rural in the city. With the help of GEE platform, we iterated over the whole process in

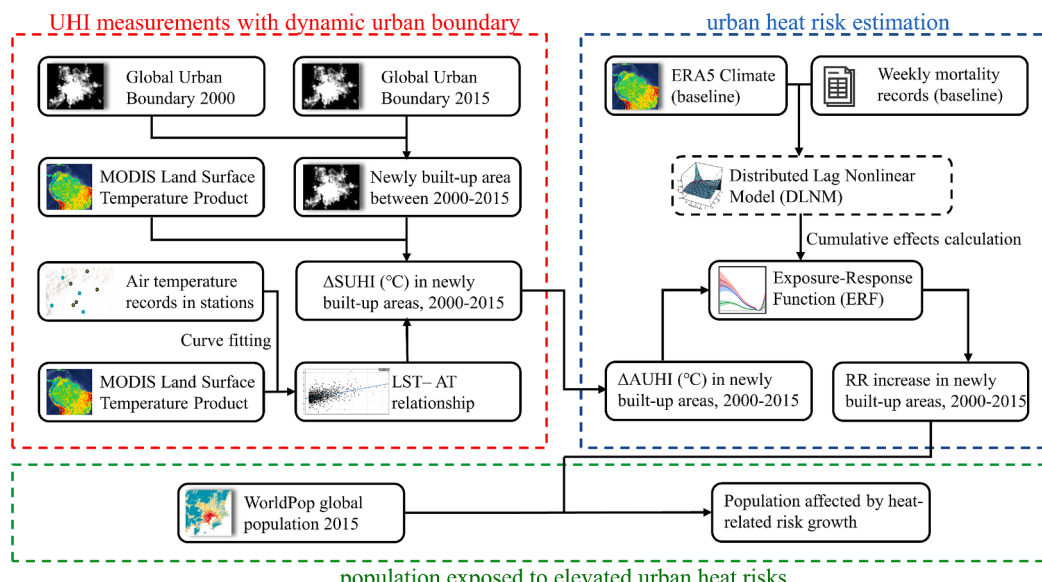


Fig. 1. Flowchart of the methodology: 1) the SUHI/AUHI measurements under the framework of dynamic urban boundary; 2) the two-stage analysis based on a DLNM model to derive relative risk; and 3) the population affected by the increased urban heat risk.

thousands of cities around the world. During 2000–2015, a total of 1,953,491 SUHI intensity records were obtained.

2.3. Quantifying excess heat risk due to urban expansion

The concept of relative risk (RR) is widely used to reflect the ratio of mortality increase when temperatures deviate from the minimum mortality temperature (MMT). When temperatures fall below or rise above MMT, the level of RR for cold or heat increases, while the RR is at its lowest (RR = 1) when the temperature is equal to the MMT. Consequently, the Exposure-Response Function (ERF) typically manifests as a U/V/J-shaped curve representing the relationship between temperature and RR (Kephart et al. 2022; Zhao et al. 2021). We adopted a two-stage analysis to establish the ERF to determine the urban heat risk (RR) in summer. In the first stage, we employed the quasi-Poisson regression with the DLNM to develop local-scale ERFs (Gasparrini et al. 2010). DLNM account for both exposure and lag dimensions and can capture the complex non-linear relationship between temperature and mortality, making them widely used in relative studies (Ballester et al. 2023; Chen et al. 2017; Gasparrini et al. 2015; Gasparrini et al. 2017; Yang et al. 2021). In our study, we utilized weekly all-cause mortality data from various countries/states provided by the STMF dataset and the U.S. CDC, alongside air temperature data from the ERA5 historical climate dataset, to construct the DLNM. This model includes an intercept, a natural cubic spline function with 8 degrees of freedom per year for time variables to control for seasonality and long-term trends, and a cross-basis function for temperature and lag duration. The temperature basis function is set as a natural cubic spline with three internal knots at the 10th, 75th, and 90th percentiles of the temperature distribution, and the lag dimension is set to 0, 1, 2, and 3 weeks. A logarithmic function is used as the link function. These parameter settings are based on standard practices in existing studies, which have demonstrated their reliability (Chen et al. 2018; Chung et al. 2015; Yang et al. 2012). The specific model formula is shown below:

$$\begin{aligned} \log(E(\text{Mort}_i)) &= NS(\text{Time}, 8\text{d.f. per year}) + \text{crossbasis}(\text{Temp}_i, \text{lag} \\ &= 0, 1, 2, 3\text{ weeks}) + b \end{aligned} \quad (4)$$

where Mort_i represents the weekly mortality observations in region i . Time is the week count vector, and Temp_i is the weekly average temperature vector. b is the intercept. After developing the DLNMs, we calculated the cumulative effects across the lag dimension to achieve dimension reduction and obtain the exposure-response curve for region i , defining the temperature at which the RR is minimized as the MMT for that region (Gasparrini and Armstrong 2013; Wang et al. 2019). In the second stage, we performed a multivariate meta-analysis on the local-scale model coefficients obtained from the first stage (Gasparrini et al. 2012). The Best Linear Unbiased Predictions were then used to refine the model coefficients, establishing the final ERF (Ballester et al. 2023; Yang et al. 2021). In regions lacking weekly mortality data, we synthesized ERFs based on other relative studies (Table S1) (Azongo et al. 2012; Dimitrova et al. 2021; Egondi et al. 2012; Gasparrini et al. 2015; Hajat et al. 2023; Kephart et al. 2022; Nguyen et al. 2023; Vicedo-Cabrera et al. 2021; Yang et al. 2021).

After obtaining the ERF, we first quantified the change in SUHI intensity in areas that experienced urban expansion between 2000 and 2015. Then, we built a linear relationship between air temperature and surface temperature at large scale to convert SUHI intensity into AUHI intensity (Table S2), since previous studies have indicated that air temperature is highly related to human heat exposure (Kloog et al. 2014; Rosenfeld et al. 2017; Shi et al. 2016). We utilized air temperature records from over 100,000 GHCN-d meteorological stations to develop linear regression models between air temperature and MODIS surface temperature data at these locations, ensuring accuracy and comprehensive global coverage by modeling each Köppen climate zone (Köppen et al. 2011) respectively (see supplementary materials for details).

Moreover, we combined calculated AUHI intensity and ERFs to estimate the corresponding change in RR. We quantified the impact of urban expansion on urban summer heat risk by calculating the percentage change in RR due to urbanization-induced warming.

$$\text{Perc} = \frac{\text{RR}' - \text{RR}}{\text{RR}} \times 100\% \quad (5)$$

We screened regions at three different Perc levels: $\text{Perc} > 10\%$, $\text{Perc} > 25\%$, and $\text{Perc} > 50\%$. Then we overlaid regions of different risk levels with the WorldPop population data and estimated the affected population in these regions by the zonal statistics. Finally, we aggregated the population covered by all urban patches under the same risk level (e.g., RR increase $> 25\%$) and divided it by the global total population to obtain the specific proportion. We chose the last year of 15 years urban expansion (2015) as the baseline year to estimate the final affected population. In line with previous studies (Gasparrini et al. 2017; Martinez-Solanas et al. 2021; Thawonmas et al. 2023), we did not account for population fluctuations to avoid introducing uncertainty. This analysis provided a global overview of the proportion of people exposed to varying degrees of heat risk as a result of urban expansion.

3. Results

3.1. Spatial and temporal dynamics of SUHI intensity in global cities from 2000 to 2015

Our statistics of SUHI results show that the dynamics of global SUHI intensity has a clear trend with diurnal patterns as well as seasonal variations. Fig. 2b shows that summer average daytime SUHI intensity globally increased from 0.78 °C in 2000 to 0.86 °C in 2015, with an increase as high as about 10.2 %. The nighttime average SUHI intensity increased from 0.45 °C in 2000 to 0.48 °C in 2015, with an increase as high as about 6.3 %. They both show a trend of steady growth in the past 15 years, although the growth rate of nighttime SUHI intensity is slightly lower than that of daytime. The difference between the box plots of the daytime and nighttime SUHI intensity in Fig. 2a-Fig. 2d shows that the nighttime SUHI intensity is more concentrated and stable compared to the daytime SUHI intensity.

Fig. 2e shows that the global daytime and nighttime SUHI intensity has a certain seasonal pattern. SUHI intensity increases continuously from winter to summer, then decreases continuously from summer to winter. Daytime SUHI intensity varies greatly with the season, with a temperature difference of up to 0.72 °C between winter and summer. Instead, nighttime SUHI intensity is more stable, with a smaller range of 0.23 °C between winter and summer. The daytime intensity is significantly higher than nighttime intensity in summer, but slightly lower in winter. However, Peng et al. (2012) found that the daytime SUHI intensity is generally higher than nighttime in 419 big cities around the world in both summer and winter. The reason for this difference probably is that Peng's research only focuses on the sample of large cities, and most of sample cities are concentrated in the temperature climate zone, which may cause a biased sampling. The results highlight the importance of ensuring adequate and unbiased sampling in large-scale SUHI research.

The results in Fig. 2e show that the SUHI effect is most significant in summer. Therefore, this study spatially visualizes the global SUHI intensity in summer (June/July/August in the northern hemisphere and December/January/February in the southern hemisphere) daytime (Fig. 3a) and nighttime (Fig. 3b) according to the locations of cities. Fig. 3a and Fig. 3b show that the spatial distribution of global daytime/nighttime SUHI intensity has both a certain degree of similarity and obvious differences. In many cities, there is significantly low daytime SUHI intensity. Instead, the nighttime SUHI intensity reaches a relatively high value, such as the Middle East, India, and Mexico (Tables S3 and S4). In 2015, the daytime SUHI intensity of cities in these areas is mostly in the range of dark green ($< -1^\circ\text{C}$) or green ($< 0^\circ\text{C}$), while the

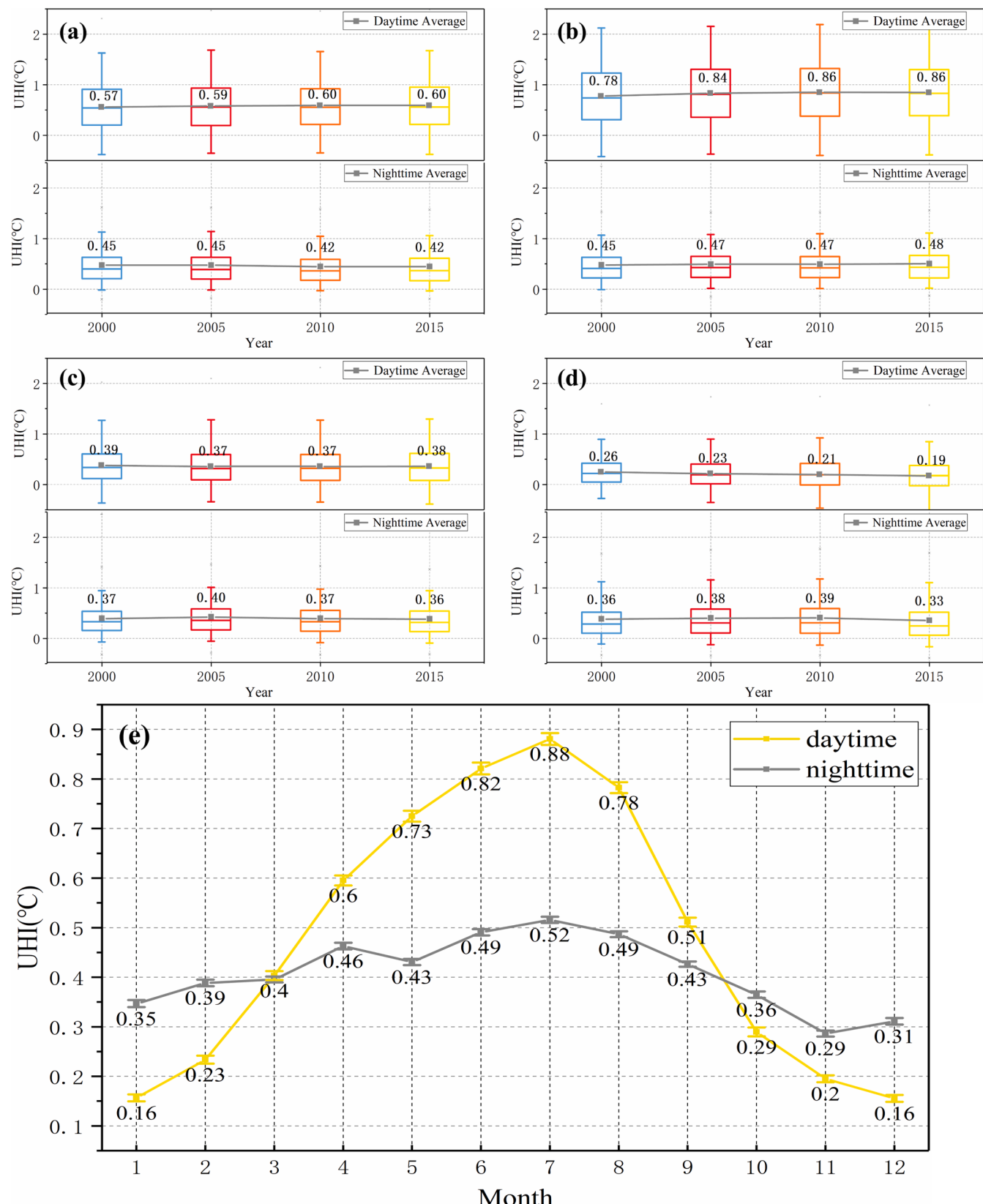


Fig. 2. Interannual variation trend of global SUHI intensity in (a) spring, (b) summer, (c) autumn, (d) winter from 2000 to 2015 and (e) monthly average intensity of global SUHI in 2015. Error bar = 1.96 Standard Error, 95 % CI.

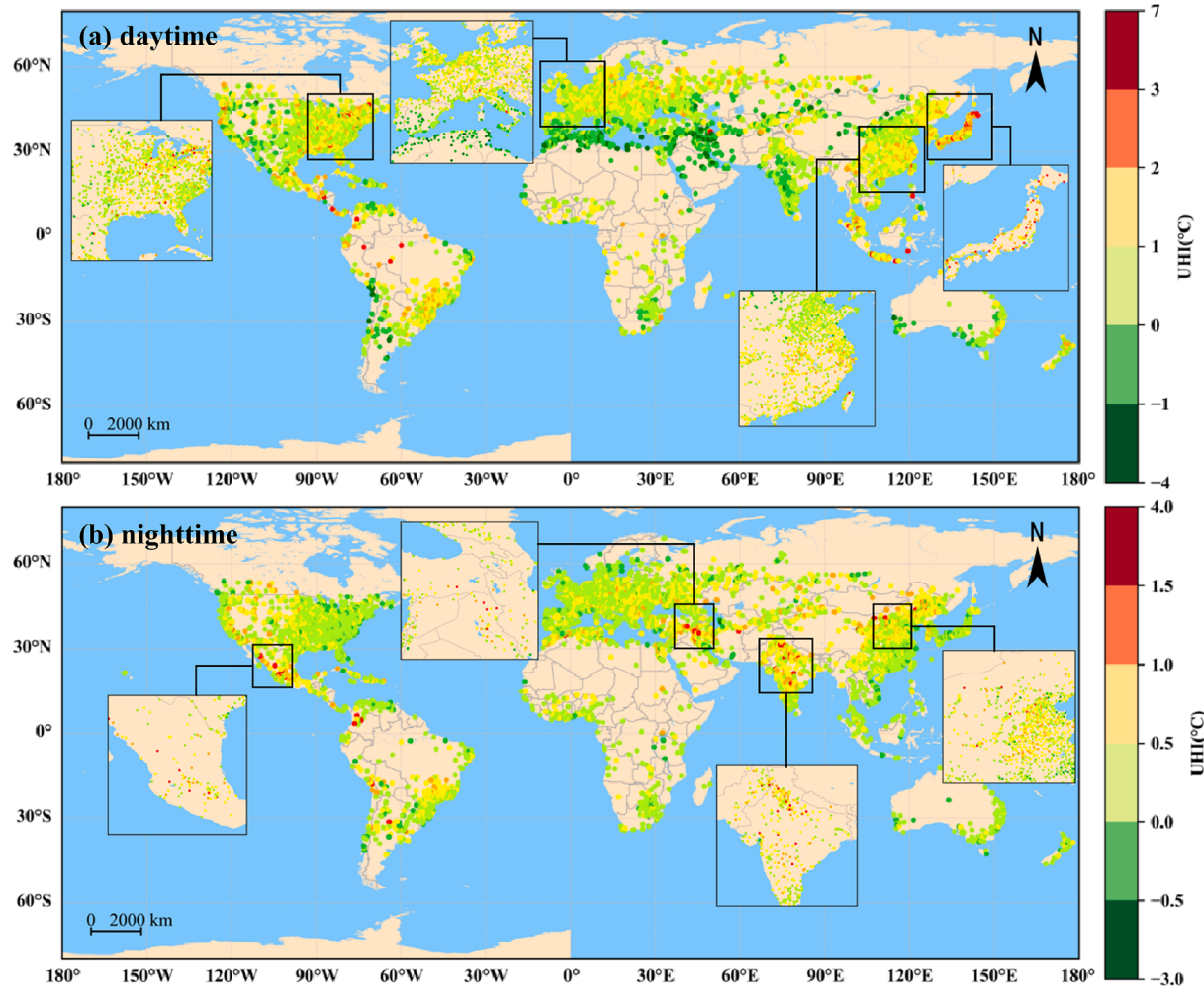


Fig. 3. (a) Global map of average daytime SUHI intensity for 7554 cities in summer 2015 derived from TERRA at 10:30 LT using the GEE platform. (b) Global map of average nighttime SUHI intensity for 7554 cities in summer 2015 derived from TERRA at 22:30 LT using the GEE platform.

nighttime SUHI intensity is in the range of orange ($> 1^{\circ}\text{C}$) or red ($> 1.5^{\circ}\text{C}$). In addition, there are some cities with high daytime SUHI intensity, but their nighttime SUHI intensity is relatively low. For example, the daytime SUHI intensity of most cities in Japan was in the red range ($> 3^{\circ}\text{C}$), while the nighttime SUHI intensity was not significant, only about $0\text{--}0.5^{\circ}\text{C}$ (in the light green range). The difference in diurnal patterns may be caused by climatic factors. In tropical, temperate, and continental climates, the daytime SUHI intensity exceeds that of the nighttime. This phenomenon is consistent with findings from numerous existing studies (Chakraborty and Lee 2019; Clinton and Gong 2013; Peng et al. 2012). In arid and semi-arid climates, the nighttime SUHI intensity is higher than that during the daytime (Fig. S1). The possible reason can be attributed to due to reduced evapotranspiration from urban vegetation. During the day, high temperatures and low humidity in the arid and semi-arid regions can lead to increased evaporation rates; however, when vegetation is stressed due to insufficient moisture, its capacity to cool the surrounding environment through evapotranspiration diminishes. As a result, urban surfaces, primarily composed of heat-retaining materials like asphalt and concrete, absorb heat during the day and release it at night, leading to elevated nighttime temperatures. Additionally, the lack of vegetation means less shade and cooling, further contributing to the higher SUHI intensity observed after sunset.

3.2. Intensification of the SUHI effect in newly built-up areas during global urban expansion

To further focus on the SUHI effect in newly built-up areas during urban expansion, we partitioned global urban and rural areas into three distinct categories. These categories encompass: *a*. Urban regions, characterized by consistently high levels of urbanization from 2000 to 2015. *b*. Rural areas, which remained rural area throughout 2000–2015 without significant urbanization. *c*. Newly built-up areas (or urbanized rural area), which were rural areas in 2000, then experienced rapid urbanization over the 15-year period and transformed into urban regions by (or before) 2015.

Fig. 4 illustrates the surface temperature variations across these three categories during 2000–2015. We observed that, for regions *a* that have been urban since 2000, their average temperature consistently maintained a relatively high level (32.08°C – 32.56°C). Conversely, for regions *b* that remained rural areas during this period, their average temperature stayed at a relatively low level (30.18°C – 30.50°C). Notably, regions *c* experienced urbanization from rural area to urban over the 15-year period displayed a gradual temperature increase (31.08°C – 32.54°C) from a moderate starting point in 2000 (slightly lower than average temperature in regions *a* but higher than in regions *b*) and approached the level of urban regions *a* by 2015.

We found that in areas that remained consistently in urban or rural throughout 2000–2015, their surface temperature also remained roughly stable at a certain high or low level. In contrast, in areas where

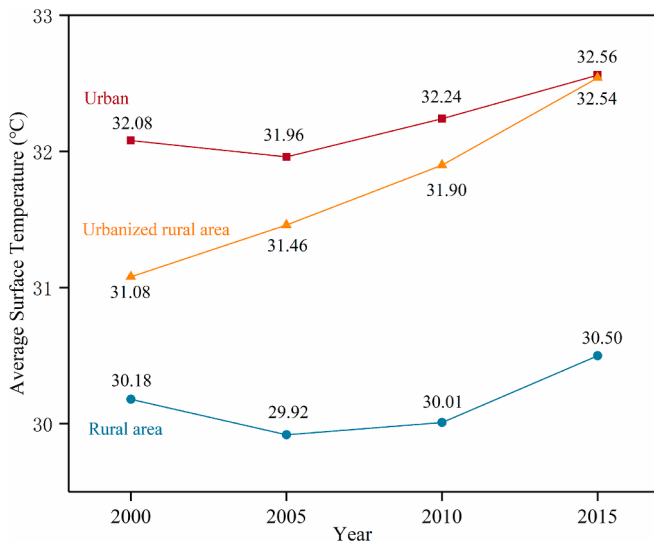


Fig. 4. Surface temperature changes every five years from 2000 to 2015 for a. Urban areas, b. Rural areas and c. Newly built-up areas (transitioning from rural areas to built-up areas during between 2000 and 2015).

urban expansion occurred, their surface temperature kept rising. And with the progress of urbanization, their surface temperature was also approaching the level of urban areas. However, due to neglecting urban expansion, the static urban boundary still considers the newly urbanized areas as rural areas around the city. Therefore, the increased rural temperature reduces the temperature difference between the urban and rural areas, leading to an underestimation of SUHI intensity, which is the reason why dynamic urban boundary are adopted in this study. In summary, Fig. 4 clearly demonstrates that while urban and rural temperatures show similar trends (attributable to background climate change), the temperatures in newly built-up areas exhibit a distinctly different pattern, gradually converging from rural to urban levels. This indicates that, driven by urban expansion, the SUHI effects in newly built-up areas became increasingly significant between 2000 and 2015.

Fig. 5 shows the change in average summer SUHI intensity in newly built-up areas globally from 2000 to 2015. Urban expansion during 2000–2015 increased the global average SUHI intensity by 0.61°C (95% CI = 0.56°C - 0.66°C) in newly built-up areas, over 1,700 cities experiencing increases of more than 2°C , while a proportion of smaller newly built-up areas did not experience pronounced SUHI effects. Cities with

large SUHI intensity growth over the 15-year period are concentrated in areas undergoing rapid urbanization (e.g. China, India, Europe). Continued increases in SUHI intensity will further affect the summer heat risk to residents of newly built-up areas, as discussed in the next section.

3.3. Increase in heat-related risk due to urban expansion

Many studies have confirmed that the SUHI effect increases the risk of urban residents' exposure to extreme heat, especially during summer daytime, leading to an increase in heat related mortality (Heaviside et al. 2016; Lowe 2016; Milojevic et al. 2016). Therefore, more and more studies have involved SUHI as an important factor in the estimation of heat related risk and death (Milojevic et al. 2011). However, driven by long-term global urban expansion, the increased heat-related risk resulting from the intensified SUHI effect in newly built-up areas, remains insufficiently quantified and studied. Here we followed the methodology mentioned in section 2.3 and calculated the percentage of RR increase (Perc) to further explore the potential impacts of global urban expansion on urban heat risk.

Due to space limitations, Fig. 6 presents the ERF for a selection of countries. Although there are variations in the MMT among countries, it generally falls within the range of 17°C to 24°C , which is the most suitable temperature for human habitation. When the air temperatures exceed the MMT, people are exposed to different degrees of high temperature risk. A steeper upward slope in the curve indicates a faster increase in heat risk with each degree Celsius rise in temperature, signifying greater vulnerability to heat. According to the ERF, the urban expansion increases summer heat risk for urban residents in two main ways. First, the urbanization-induced warming leads to more days with average air temperatures exceeding the MMT, resulting in prolonged exposure to heat-related risk in summer. Second, the urbanization-induced warming increases the magnitude of urban daily temperatures above the MMT, exposing people to stronger heat risks in summer.

Fig. 7 shows the changes in RR caused by urban expansion globally from 2000 to 2015. Our statistics of Fig. 7 indicates that between 2000 and 2015, the urban expansion led to a 20 % (95 % CI = 14.8 %-25.2 %) increase in global average summer heat-related risk. This means that urbanization results in an additional 20 % (95 % CI = 14.8 %-25.2 %) of heat-related deaths annually in newly built-up areas worldwide. Fig. 7 shows that the increase in urban heat risk due to urbanization-induced warming is notably higher in regions such as East China, India, and Europe, generally exceeding 50 %, which is close to the results in Europe (~45 %) reported by Huang et al. (2023). These countries should pay

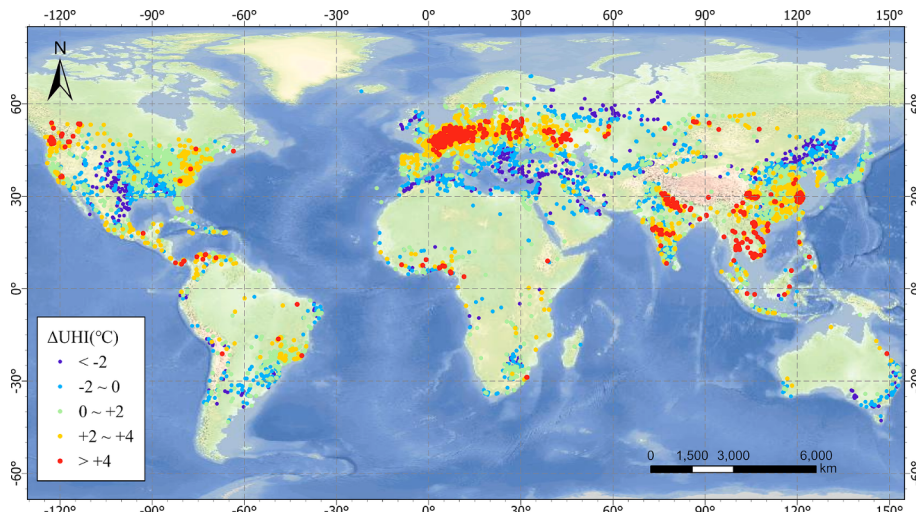


Fig. 5. Changes in average summer SUHI intensity ($^{\circ}\text{C}$) in newly built-up areas globally from 2000 to 2015.

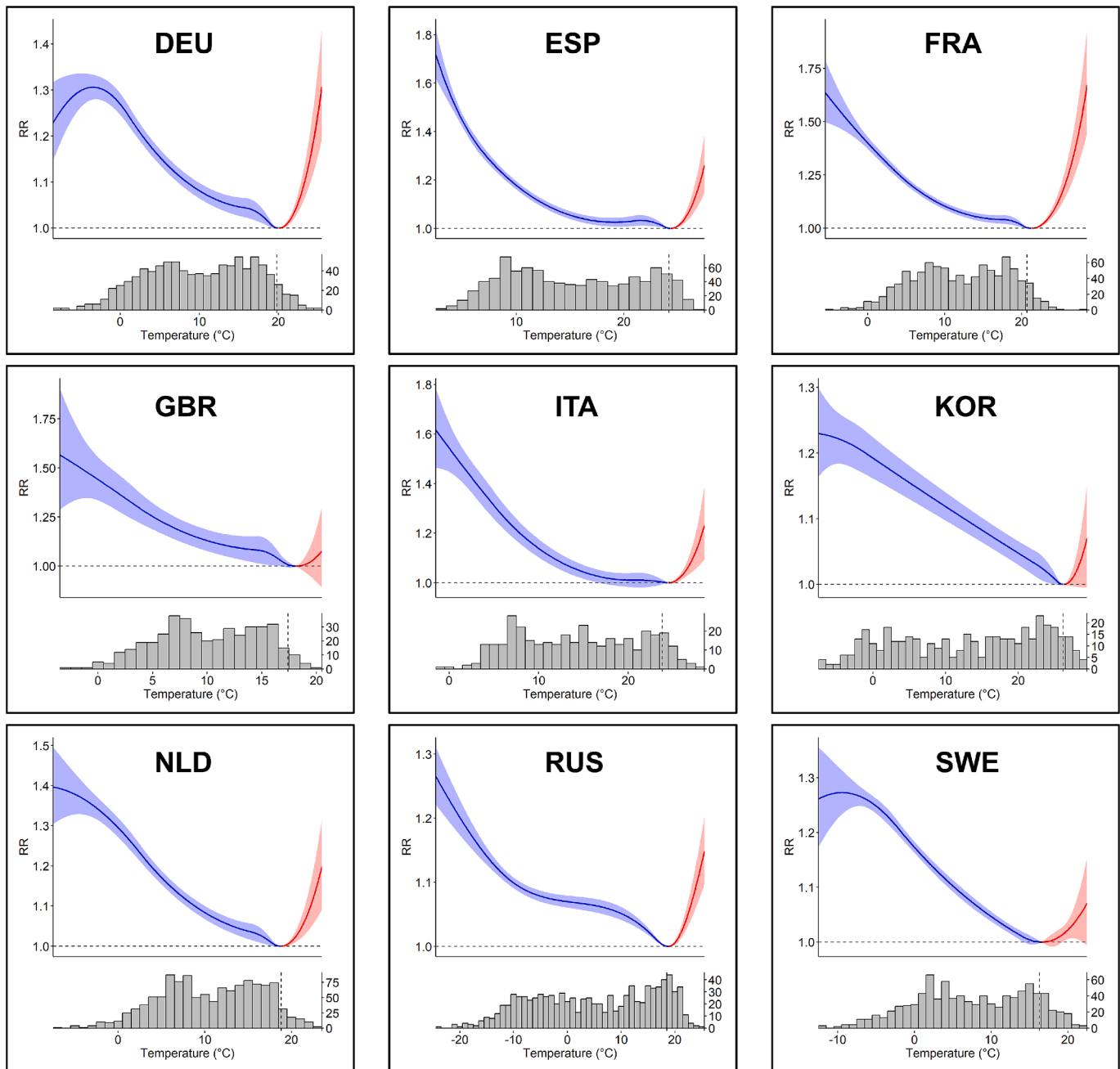


Fig. 6. Country-level ERF derived from the two-stage analysis based on DLNM. The abbreviations in the figure correspond to the following countries: DEU-Germany, ESP-Spain, FRA-France, GBR-United Kingdom, ITA-Italy, KOR-South Korea, NLD-Netherlands, RUS-Russia, SWE-Sweden.

close attention to the urbanization-induced warming. Particularly in countries where the ERF function indicates higher vulnerability to heat risk, even a modest increase in temperature can lead to severe heat-related mortality. Therefore, alongside urban development in these regions, it is essential to plan for urban green spaces or implement other measures to mitigate SUHI and AUHI impacts. After combining world population data 2015 (Lloyd et al. 2019) to calculate the number of urban residents involved in RR increase, We found that about 4 % of the global population (~287 million) experienced varying increases in heat-related risk during 2000–2015 due to the urban expansion. And the population with the percentage change in RR (*Perc*) $> 10\%$ accounted for about 2.3 % (~170 million) of the global population. Besides, there were 1 % (~78 million) of the global population with *Perc* greater than 25 %, even 0.21 % of the global population (~15 million) with *Perc* greater than 50 %. Although this is an approximate estimation based on

very limited available data, it still reveals the fact that urban expansion may lead to significant increase of RR, and considering the large size global urban population, the future extreme heat risks of millions of residents are likely to exceed existing projections. Governments should develop more targeted policies for rapidly urbanization areas to reduce the local heat risk.

4. Discussions and Conclusions

In this study, we conducted the study of global SUHI effect based on the dynamic urban boundary and MODIS surface temperature data. Firstly, we extracted every five-year dynamic urban boundary and measured the SUHI intensity of over 7,500 urban patches with the urban size larger than 10 km^2 worldwide from 2000 to 2015 with the help of GEE platform. The analysis yielded the temporal variation and spatial

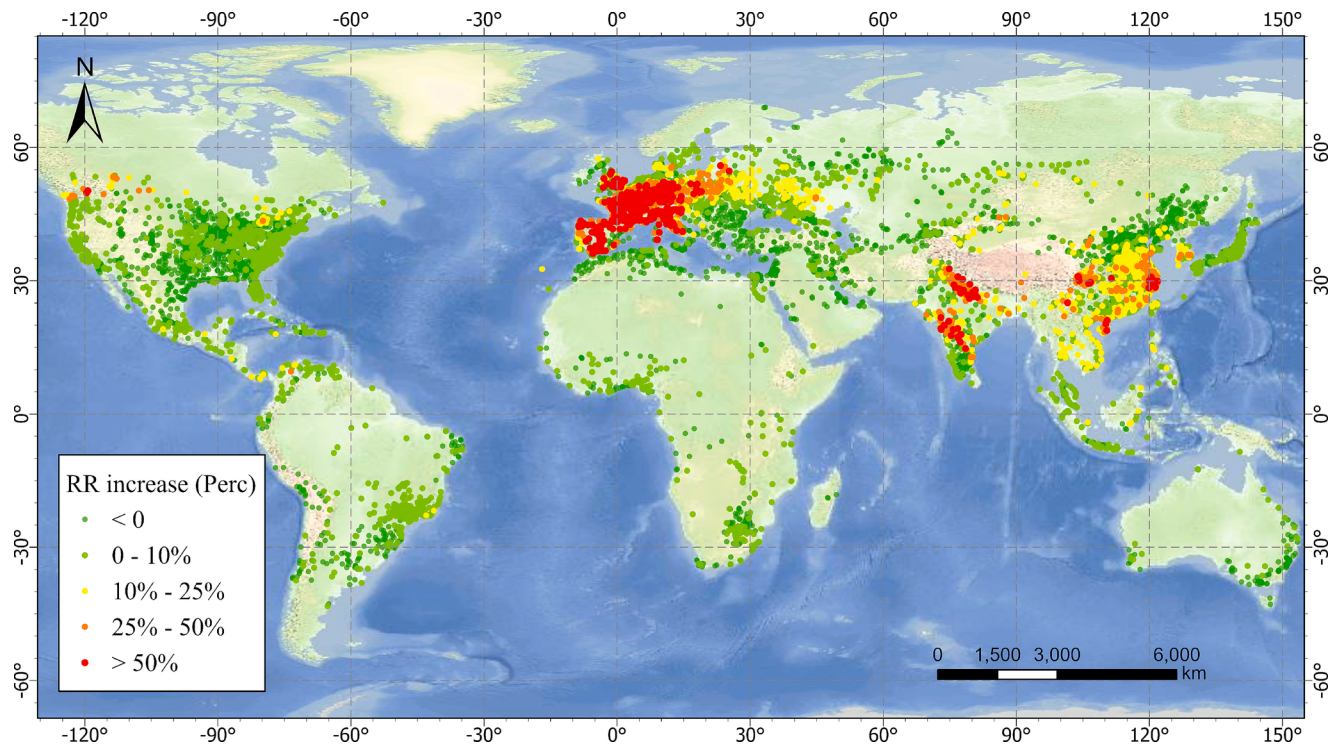


Fig. 7. Changes in average summer RR due to urban expansion globally from 2000 to 2015.

distribution of SUHI intensity in these cities. We then quantified the urbanization-induced warming in regions that underwent urban expansion from 2000 to 2015. Finally, we further estimated the higher urban heat risk reflected by the urbanization-induced warming through a two-stage analysis based on the DLNM.

We found that the global SUHI intensity shows a steady growth trend from 2000 to 2015, with a 10.2 % increase in daytime SUHI intensity. In addition, the SUHI intensity also shows the seasonal variation of increase in summer and decrease in winter. Daytime SUHI intensity is higher than nighttime SUHI intensity in summer, but lower in winter. Affected by the climate, the spatial distribution of nighttime SUHI intensity is significantly different from that in daytime, which is reflected in that many cities with high/low daytime SUHI intensity have low/high nighttime SUHI intensity, such as some cities in Middle East, Mexico and Japan.

The advantage of adopting dynamic urban boundary allowed us to focus on the newly built-up areas during urban expansion, which previous studies have often overlooked. We found that surface temperatures in urban/rural areas generally stabilized at a higher/lower level and follow the same trend over the period 2000–2015. In contrast, newly built-up areas showed a very different pattern, with SUHI intensity gradually transitioning from the rural level to the urban level during 2000–2015, which demonstrates that the SUHI effect intensifies as newly built-up areas transition from natural vegetation to impervious surfaces driven by urban expansion.

Our results reveal that urban expansion led to average 0.61°C (95 % CI = 0.56°C–0.66°C) increase in summer SUHI intensity in newly built-up areas globally from 2000 to 2015. The urbanization-induced warming further resulted in an average 20 % increase in urban heat risks, which implies an additional 20 % (95 % CI = 14.8 %–25.2 %) in heat-related mortality annually in newly built-up areas. Moreover, we found that due to urban expansion, over 2.3 % of the global population faces more than a 10 % increase in heat-related risks, while 1 % of the population faces an increase exceeding 25 %, with ~ 15 million people experiencing a risk increase of more than 50 %. These results underscore the significant potential impact of urban expansion on urban

temperature elevation and urban heat-related risks. Given the ongoing global urbanization process, future summer heat risk may exceed current projections. To reduce the impact of urban expansion, various strategies can be implemented. Several studies report that increasing urban greening (Pace et al. 2022). Additionally, cool pavement and cool roof initiatives, which aim to increase the reflectivity of roofs and pavements, can decrease temperatures for increase in reflectivity (Santamouris et al. 2017; Santamouris and Fiorito 2021). Green roof measures (vegetation on rooftops) are also beneficial in mitigating the UHI effect (Santamouris and Fiorito 2021).

This study is of great significance for illustrating the distribution and variation of global SUHI intensity under dynamic urban boundary. More importantly, this study contributes to the quantification of heat-related risks exacerbated by urbanization-induced warming in newly built-up areas with a deeper understanding of the role of urban expansion dynamics. However, for many existing studies, there remains a gap in understanding SUHI as a dynamic variable influenced by large-scale urban expansion. For example, Jungman et al. (2023) fixed SUHI intensity at 2015 levels in their study of heat risks in European cities, and Huang et al. (2023) fixed it at 2012 levels without considering urban expansion. In contrast, our research addresses the dynamic changes in SUHI intensity associated with newly built-up urban areas during ongoing urban expansion, thereby filling a critical gap in the existing literature. Moreover, our study includes over 7,500 cities worldwide, making the results valuable on a global scale, which is equally significant. Even though some existing studies do consider the dynamic changes of SUHI intensity during urban expansion, they often focus on a limited scale and, therefore, cannot provide globally applicable insights. For instance, Hondula et al. (2014) found that urban expansion from 1983 to 2007 in Maricopa County (USA) led to a 359 % increase in heat risk, and Wicki et al. (2024) reported a 31 % increase in heat risk in eight Swiss cities due to urban expansion from 2003 to 2016. However, the limited sample of these studies restricts their global relevance. Our research addresses these limitations by offering a more comprehensive analysis applicable on a global scale. In comparison to the local-scale results mentioned above, our findings reveal a global pattern of urban

expansion's impact on heat-related risks, highlighting a north–south inequality (Fig. 7). Specifically, the increase in heat-related risks due to urban expansion is greater in the Northern Hemisphere than in the Southern Hemisphere. Consequently, newly built-up urban areas in the north have a more urgent need for measures to mitigate the SUHI effect compared to those in the south.

However, there are three limitations in this study. First, we treated the urban interior as a homogeneous impervious surface, which ignores both the stronger SUHI effect in densely built-up areas of the city and the mitigation effect of city green spaces on SUHI. Future study will focus on the spatial heterogeneity of SUHI intensity in the interior of the city. Further grading urban areas based on impervious surface density and calculating the SUHI intensity separately for each category is a feasible approach. Second, in order to avoid introducing uncertainty, the study did not consider population fluctuations. Future research will take population dynamics into account to exhibit the affected populations across different years by the newly built-up areas. Third, the relationship between air temperature and mortality (or RR) is based on the very limited data available to us, and may not remain precise at a regional scale. In the future, we will attempt to use variables such as GDP to perform multivariate *meta*-regression, which aims to establish an ERF based on limited data while aligning as closely as possible with the region's actual conditions.

CRediT authorship contribution statement

Ming Hao: Writing – review & editing, Writing – original draft, Visualization, Validation, Software, Methodology, Investigation, Data curation. **Xue Liu:** Writing – review & editing, Supervision, Project administration, Funding acquisition. **Xia Li:** Writing – review & editing, Supervision, Funding acquisition, Conceptualization.

Declaration of competing interest

The authors declare that they have no known competing financial interests or personal relationships that could have appeared to influence the work reported in this paper.

Acknowledgements

This work was supported by the National Natural Science Foundation of China (Grant No. 42130107, 42201309), the Youth Project of the Humanities and Social Sciences of Chinese Ministry of Education (No. 22YJCZH113), and the Science and Technology Commission of Shanghai Municipality (No. 22YF1410900).

Appendix A. Supplementary data

Supplementary data to this article can be found online at <https://doi.org/10.1016/j.jag.2024.104344>.

Data availability

Data will be made available on request.

References

- Abrar, R., Sarkar, S.K., Nishtha, K.T., Talukdar, S., Shahfahad, Rahman, A., Islam, A.R.M. T., & Mosavi, A. (2022). Assessing the spatial mapping of heat vulnerability under urban heat island (UHI) effect in the dhaka metropolitan area. *Sustainability*, 14, 4945.
- Arnfield, A.J., 2003. Two decades of urban climate research: a review of turbulence, exchanges of energy and water, and the urban heat island. *Int. J. Climatol.* 23, 1–26.
- Azongo, D.K., Awine, T., Wak, G., Binka, F.N., & Rexford Oduro, A. (2012). A time series analysis of weather variables and all-cause mortality in the Kasena-Nankana Districts of Northern Ghana, 1995–2010. *Global Health Action*, 5.
- Ballester, J., Quijal-Zamorano, M., Mendez Turribiates, R.F., Pegenauta, F., Herrmann, F.R., Robine, J.M., Basagana, X., Tonne, C., Anto, J.M., Achebak, H., 2023. Heat-related mortality in Europe during the summer of 2022. *Nat. Med.* 29, 1857–1866.
- Carroll, M., C. DiMiceli, M. Wooten, A. Hubbard, R. Sohlberg, J. Townshend. (2017). MOD44W MODIS/Terra Land Water Mask Derived from MODIS and SRTM L3 Global 250m SIN Grid V006.
- Centers for Disease Control and Prevention, N.C.f.H.S. (2018–2021). Provisional Mortality on CDC WONDER Online Database. In N.V.S. System (Ed.).
- Chakraborty, T., Lee, X., 2019. A simplified urban-extent algorithm to characterize surface urban heat islands on a global scale and examine vegetation control on their spatiotemporal variability. *Int. J. Appl. Earth Obs. Geoinf.* 74, 269–280.
- Chen, K., Horton, R.M., Bader, D.A., Lesk, C., Jiang, L., Jones, B., Zhou, L., Chen, X., Bi, J., Kinney, P.L., 2017. Impact of climate change on heat-related mortality in Jiangsu Province, China. *Environ. Pollut.* 224, 317–325.
- Chen, R., Yin, P., Wang, L., Liu, C., Niu, Y., Wang, W., Jiang, Y., Liu, Y., Liu, J., Qi, J., 2018. Association between ambient temperature and mortality risk and burden: time series study in 272 main Chinese cities. *BMJ* 363.
- Chung, Y., Lim, Y.-H., Honda, Y., Guo, Y.-L.-L., Hashizume, M., Bell, M.L., Chen, B.-Y., Kim, H., 2015. Mortality related to extreme temperature for 15 cities in northeast Asia. *Epidemiology* 26, 255–262.
- CIESIN - Columbia University (2016). Global Urban Heat Island (UHI) Data Set, 2013. In. Palisades, New York: NASA Socioeconomic Data and Applications Center (SEDAC).
- Clinton, N., Gong, P., 2013. MODIS detected surface urban heat islands and sinks: Global locations and controls. *Remote Sens. Environ.* 134, 294–304.
- Dimitrova, A., Ingole, V., Basagana, X., Ranzani, O., Mila, C., Ballester, J., Tonne, C., 2021. Association between ambient temperature and heat waves with mortality in South Asia: Systematic review and meta-analysis. *Environ. Int.* 146, 106170.
- Egondi, T., Kyobutungi, C., Kovats, S., Muindi, K., Ettarh, R., Rocklöv, J., 2012. Time-series analysis of weather and mortality patterns in Nairobi's informal settlements. *Glob. Health Action* 5.
- Elmqvist, T., Fragkias, M., Goodness, J., Güneralp, B., Marcotullio, P.J., McDonald, R.I., Parnell, S., Schewenius, M., Sendstad, M., Seto, K.C., 2013. Urbanization, biodiversity and ecosystem services: challenges and opportunities: a global assessment. *Springer Nature*.
- Fu, X., Yao, L., Sun, S., 2022. Assessing the heat exposure risk in Beijing–Tianjin–Hebei region based on heat island footprint analysis. *Atmos.* 13, 739.
- Gaffin, S., Rosenzweig, C., Khanbilvardi, R., Parshall, L., Mahani, S., Clickman, H., Goldberg, R., Blake, R., Slosberg, R., Hillel, D., 2008. Variations in New York City's urban heat island strength over time and space. *Theor. Appl. Climatol.* 94, 1–11.
- Gasparri, A., Armstrong, B., 2013. Reducing and meta-analysing estimates from distributed lag non-linear models. *BMC Med. Res. Method.* 13, 1–10.
- Gasparri, A., Armstrong, B., Kenward, M.G., 2010. Distributed lag non-linear models. *Stat. Med.* 29, 2224–2234.
- Gasparri, A., Armstrong, B., Kenward, M.G., 2012. Multivariate meta-analysis for non-linear and other multi-parameter associations. *Stat. Med.* 31, 3821–3839.
- Gasparri, A., Guo, Y., Sera, F., Vicedo-Cabrera, A.M., Huber, V., Tong, S., Coelho, M.d. S.Z.S., Saldiva, P.H.N., Lavigne, E., & Correa, P.M. (2017). Projections of temperature-related excess mortality under climate change scenarios. *The Lancet Planetary Health*, 1, e360–e367.
- Gasparri, A., Guo, Y., Hashizume, M., Lavigne, E., Zanobetti, A., Schwartz, J., Tobias, A., Tong, S., Rocklöv, J., Forsberg, B., 2015. Mortality risk attributable to high and low ambient temperature: a multicountry observational study. *Lancet* 386, 369–375.
- Hajat, S., Proestos, Y., Araya-Lopez, J.-L., Economou, T., Lelieveld, J., 2023. Current and future trends in heat-related mortality in the MENA region: a health impact assessment with bias-adjusted statistically downscaled CMIP6 (SSP-based) data and Bayesian inference. *Lancet Planet. Health* 7, e282–e290.
- Heavyside, C., Vardoulakis, S., Cai, X.-M., 2016. Attribution of mortality to the urban heat island during heatwaves in the West Midlands, UK. *Environ. Health* 15, 49–59.
- Hersbach, H., Bell, B., Berrisford, P., Hirahara, S., Horányi, A., Muñoz-Sabater, J., Nicolas, J., Peubey, C., Radu, R., Schepers, D., 2020. The ERA5 global reanalysis. *Q. J. R. Meteorol. Soc.* 146, 1999–2049.
- Ho, J.Y., Shi, Y., Lau, K.K., Ng, E.Y., Ren, C., Goggins, W.B., 2023. Urban heat island effect-related mortality under extreme heat and non-extreme heat scenarios: A 2010–2019 case study in Hong Kong. *Sci. Total Environ.* 858, 159791.
- Hondula, D.M., Georgescu, M., Balling, R.C., 2014. Challenges associated with projecting urbanization-induced heat-related mortality. *Sci. Total Environ.* 490, 538–544.
- Huang, K.N., Li, X., Liu, X.P., Seto, K.C., 2019. Projecting global urban land expansion and heat island intensification through 2050. *Environ. Res. Lett.* 14.
- Huang, W.T.K., Masselot, P., Bou-Zeid, E., Fatichi, S., Paschalidis, A., Sun, T., Gasparri, A., Manoli, G., 2023. Economic valuation of temperature-related mortality attributed to urban heat islands in European cities. *Nat. Commun.* 14.
- Imhoff, M.L., Zhang, P., Wolfe, R.E., Bouyoua, L., 2010. Remote sensing of the urban heat island effect across biomes in the continental USA. *Remote Sens. Environ.* 114, 504–513.
- Iungman, T., Cirach, M., Marando, F., Pereira Barboza, E., Khomenko, S., Masselot, P., Quijal-Zamorano, M., Mueller, N., Gasparri, A., Urquiza, J., Heris, M., Thondoo, M., Nieuwenhuijsen, M., 2023. Cooling cities through urban green infrastructure: a health impact assessment of European cities. *Lancet* 401, 577–589.
- Jdanov, D.A., Galarza, A.A., Shkolnikov, V.M., Jasilionis, D., Németh, L., Leon, D.A., Boe, C., Barbieri, M., 2021. The short-term mortality fluctuation data series, monitoring mortality shocks across time and space. *Sci. Data* 8, 235.
- Kephart, J.L., Sánchez, B.N., Moore, J., Schinasi, L.H., Bakhtiyarava, M., Ju, Y., Gouveia, N., Caiaffa, W.T., Dronova, I., Arunachalam, S., 2022. City-level impact of extreme temperatures and mortality in Latin America. *Nat. Med.* 28, 1700–1705.
- Kim, S.W., Brown, R.D., 2021. Urban heat island (UHI) variations within a city boundary: A systematic literature review. *Renew. Sustain. Energy Rev.* 148, 111256.

- Kloog, I., Nordio, F., Coull, B.A., Schwartz, J., 2014. Predicting spatiotemporal mean air temperature using MODIS satellite surface temperature measurements across the Northeastern USA. *Remote Sens. Environ.* 150, 132–139.
- Kolokotroni, M., Giridharan, R., 2008. Urban heat island intensity in London: An investigation of the impact of physical characteristics on changes in outdoor air temperature during summer. *Sol. Energy* 82, 986–998.
- Köppen, W., Volken, E., Brönnimann, S., 2011. The thermal zones of the earth according to the duration of hot, moderate and cold periods and to the impact of heat on the organic world (Translated from: Die Wärmezonen der Erde, nach der Dauer der heissen, gemässigten und kalten Zeit und nach der Wirkung der Wärme auf die organische Welt betrachtet). *Meteorol. Z.* 20, 351–360.
- Li, X.C., Gong, P., Zhou, Y.Y., Wang, J., Bai, Y.Q., Chen, B., Hu, T.Y., Xiao, Y.X., Xu, B., Yang, J., Liu, X.P., Cai, W.J., Huang, H.B., Wu, T.H., Wang, X., Lin, P., Li, X., Chen, J., He, C.Y., Li, X., Yu, L., Clinton, N., Zhu, Z.L., 2020. Mapping global urban boundaries from the global artificial impervious area (GAIA) data. *Environ. Res. Lett.* 15.
- Li, L., Zhan, W., Hu, L., Chakraborty, T., Wang, Z., Fu, P., Wang, D., Liao, W., Huang, F., Fu, H., 2023. Divergent urbanization-induced impacts on global surface urban heat island trends since 1980s. *Remote Sens. Environ.* 113650.
- Li, M., Zhou, B.-B., Gao, M., Chen, Y., Hao, M., Hu, G., Li, X., 2022. Spatiotemporal dynamics of global population and heat exposure (2020–2100): Based on improved SSP-consistent population projections. *Environ. Res. Lett.* 17, 094007.
- Liao, W., Wang, D., Liu, X., Wang, G., Zhang, J., 2017. Estimated influence of urbanization on surface warming in Eastern China using time-varying land use data. *Int. J. Climatol.* 37, 3197–3208.
- Liao, W., Liu, X., Li, D., Luo, M., Wang, D., Wang, S., Baldwin, J., Lin, L., Li, X., Feng, K., Hubacek, K., Yang, X., 2018. Stronger Contributions of Urbanization to Heat Wave Trends in Wet Climates. *Geophys. Res. Lett.* 45.
- Liu, X., Zhou, Y., Yue, W., Li, X., Liu, Y., Lu, D., 2020. Spatiotemporal patterns of summer urban heat island in Beijing, China using an improved land surface temperature. *J. Clean. Prod.* 257.
- Liu, X., Ming, Y., Liu, Y., Yue, W., Han, G., 2022a. Influences of landform and urban form factors on urban heat island. In: Comparative Case Study between Chengdu and Chongqing. *Science of the Total Environment*, p. 820.
- Liu, Z., Zhan, W., Bechtel, B., Voogt, J., Lai, J., Chakraborty, T., Wang, Z.-H., Li, M., Huang, F., Lee, X., 2022b. Surface warming in global cities is substantially more rapid than in rural background areas. *Commun. Earth Environ.* 3, 219.
- Lloyd, C.T., Chamberlain, H., Kerr, D., Yetman, G., Pistolesi, L., Stevens, F.R., Gaughan, A.E., Nieves, J.J., Hornby, G., MacManus, K., 2019. Global spatio-temporally harmonised datasets for producing high-resolution gridded population distribution datasets. *Big Earth Data* 3, 108–139.
- Lowe, S.A., 2016. An energy and mortality impact assessment of the urban heat island in the US. *Environ. Impact Assess. Rev.* 56, 139–144.
- Manoli, G., Fatichi, S., Schläpfer, M., Yu, K., Crowther, T.W., Meili, N., Burlando, P., Katul, G.G., Bou-Zeid, E., 2019. Magnitude of urban heat islands largely explained by climate and population. *Nature* 573, 55–60.
- Martinez-Solanas, E., Quijal-Zamorano, M., Achebak, H., Petrova, D., Robine, J.M., Herrmann, F.R., Rodo, X., Ballester, J., 2021. Projections of temperature-attributable mortality in Europe: a time series analysis of 147 contiguous regions in 16 countries. *Lancet Planet Health* 5, e446–e454.
- Menne, M.J., Durre, I., Vose, R.S., Gleason, B.E., Houston, T.G., 2012. An overview of the global historical climatology network-daily database. *J. Atmos. Oceanic Tech.* 29, 897–910.
- Milojevic, A., Wilkinson, P., Armstrong, B., Davis, M., Mavrogiani, A., Bohnenstengel, S., Belcher, S., 2011. Impact of London's urban heat island on heat-related mortality. *Epidemiology* 22, S182–S183.
- Milojevic, A., Armstrong, B.G., Gasparrini, A., Bohnenstengel, S.I., Barratt, B., Wilkinson, P., 2016. Methods to estimate acclimatization to urban heat island effects on heat-and cold-related mortality. *Environ. Health Perspect.* 124, 1016–1022.
- Mohan, M., Kikegawa, Y., Gurjar, B., Bhati, S., Kolli, N.R., 2013. Assessment of urban heat island effect for different land use-land cover from micrometeorological measurements and remote sensing data for megacity Delhi. *Theor. Appl. Climatol.* 112, 647–658.
- Nguyen, C.V., Nguyen, M.H., Nguyen, T.T., 2023. The impact of cold waves and heat waves on mortality: Evidence from a lower middle-income country. *Health Econ.* 32, 1220–1243.
- Oke, T.R., 2002. Boundary layer climates. Routledge.
- Osserman, R., 1978. The isoperimetric inequality. *Bull. Am. Math. Soc.* 84, 1182–1238.
- Pace, R., Chiocchini, F., Sarti, M., Endreny, T.A., Calfapietra, C., Ciolfi, M., 2022. Integrating Copernicus land cover data into the i-Tree Cool Air model to evaluate and map urban heat mitigation by tree cover. *European Journal of Remote Sensing* 56.
- Pappalardo, S.E., Zanetti, C., Todeschi, V., 2023. Mapping urban heat islands and heat-related risk during heat waves from a climate justice perspective: A case study in the municipality of Padua (Italy) for inclusive adaptation policies. *Landsc. Urban Plan.* 238, 104831.
- Peng, S., Piao, S., Ciais, P., Friedlingstein, P., Ottle, C., Breon, F.M., Nan, H., Zhou, L., Myneni, R.B., 2012. Surface urban heat island across 419 global big cities. *Environ. Sci. Technol.* 46, 696–703.
- Phelan, P.E., Kaloush, K., Miner, M., Golden, J., Phelan, B., Silva, H., Taylor, R.A., 2015. Urban Heat Island: Mechanisms, Implications, and Possible Remedies. *Annu. Rev. Env. Resour.* 40 (40), 285–307.
- Rosenfeld, A., Dorman, M., Schwartz, J., Novack, V., Just, A.C., Kloog, I., 2017. Estimating daily minimum, maximum, and mean near surface air temperature using hybrid satellite models across Israel. *Environ. Res.* 159, 297–312.
- Santamouris, M., Ding, L., Fiorito, F., Oldfield, P., Osmond, P., Paolini, R., Prasad, D., Synnefa, A., 2017. Passive and active cooling for the outdoor built environment – Analysis and assessment of the cooling potential of mitigation technologies using performance data from 220 large scale projects. *Sol. Energy* 154, 14–33.
- Santamouris, M., Fiorito, F., 2021. On the impact of modified urban albedo on ambient temperature and heat related mortality. *Sol. Energy* 216, 493–507.
- Sharifi, E., Lehmann, S., 2014. Comparative analysis of surface urban heat island effect in central Sydney. *Journal of Sustainable Development* 7, 23–24.
- Shastri, H., Barik, B., Ghosh, S., Venkataraman, C., Sadavarte, P., 2017. Flip flop of Day-night and Summer-Winter Surface Urban Heat Island Intensity in India. *Sci Rep* 7, 40178.
- Shi, L., Liu, P., Kloog, I., Lee, M., Kosheleva, A., Schwartz, J., 2016. Estimating daily air temperature across the Southeastern United States using high-resolution satellite data: A statistical modeling study. *Environ. Res.* 146, 51–58.
- Si, M., Li, Z.-L., Nerry, F., Tang, B.-H., Leng, P., Wu, H., Zhang, X., Shang, G., 2022. Spatiotemporal pattern and long-term trend of global surface urban heat islands characterized by dynamic urban-extent method and MODIS data. *ISPRS J. Photogramm. Remote Sens.* 183, 321–335.
- Stewart, I.D., 2011. A systematic review and scientific critique of methodology in modern urban heat island literature. *Int. J. Climatol.* 31, 200–217.
- Stone Jr, B., 2007. Urban and rural temperature trends in proximity to large US cities: 1951–2000. *Int. J. Climatol.* 27, 1801–1807.
- Thawonmas, R., Hashizume, M., Kim, Y., 2023. Projections of temperature-related suicide under climate change scenarios in Japan. *Environ Health Perspect.* 131, 117012.
- Tran, H., Uchihama, D., Ochi, S., Yasuoka, Y., 2006. Assessment with satellite data of the urban heat island effects in Asian mega cities. *Int. J. Appl. Earth Obs. Geoinf.* 8, 34–48.
- United Nations, D.o.E.a.S.A, 2019. World Urbanization Prospects: The 2018 Revision. In: United Nations, New York.
- Vicedo-Cabrera, A.M., Scovronick, N., Sera, F., Royé, D., Schneider, R., Tobias, A., Astrom, C., Guo, Y., Honda, D.M., Abrutzky, R., Tong, S., Coelho, M.d.S., Z.S., Saldiva, P.H.N., Lavigne, E., Correa, P.M., Ortega, N.V., Kan, H., Osorio, S., Kysely, J., Urban, A., Orru, H., Indermitte, E., Jaakkola, J.J.K., Ryti, N., Pascal, M., Schneider, A., Katsouyanni, K., Samoli, E., Mayvaneh, F., Entezari, A., Goodman, P., Zeka, A., Michelozzi, P., de' Donato, F., Hashizume, M., Ahmad, B., Diaz, M.H., Valencia, C.D.L.C., Overcenco, A., Houthuijs, D., Ameling, C., Rao, S., Di Ruscio, F., Carrasco-Escobar, G., Seposo, X., Silva, S., Madureira, J., Holobaca, I.H., Fratianni, S., Acquaotta, F., Kim, H., Lee, W., Iniguez, C., Forsberg, B., Ragettli, M.S., Guo, Y.L., Chen, B.Y., Li, S., Armstrong, B., Aleman, A., Zanobetti, A., Schwartz, J., Dang, T., Dung, D.V., Gillett, N., Haines, A., Mengel, M., Huber, V., & Gasparrini, A., (2021). The burden of heat-related mortality attributable to recent human-induced climate change. *Nature climate change*, 11, 492–500.
- Voogt, J.A., Oke, T.R., 2003. Thermal remote sensing of urban climates. *Remote Sens. Environ.* 86, 370–384.
- Voogt, J. (2007). How researchers measure urban heat islands. In, United States Environmental Protection Agency (EPA), State and Local Climate and Energy Program, Heat Island Effect, Urban Heat Island Webcasts and Conference Calls.
- Wan, Z., Hook, S., Hulley, G. (2015). MOD11A2 MODIS/Terra Land Surface Temperature/Emissivity 8-Day L3 Global 1km SIN Grid V006 In N.E.L.P.D.A.A. Center (Ed.).
- Wang, Z., Liu, M., Liu, X., Meng, Y., Zhu, L., Rong, Y., 2020. Spatio-temporal evolution of surface urban heat islands in the Chang-Zhu-Tan urban agglomeration. *Physics and Chemistry of the Earth, Parts a/b/c* 117, 102865.
- Wang, Y.J., Wang, A.Q., Zhai, J.Q., Tao, H., Jiang, T., Su, B.D., Yang, J., Wang, G.J., Liu, Q.Y., Gao, C., Kundzewicz, Z.W., Zhan, M.J., Feng, Z.Q., Fischer, T., 2019. Tens of thousands additional deaths annually in cities of China between 1.5 degrees C and 2.0 degrees C warming. *Nat. Commun.* 10, 1–7.
- Wicki, B., Flückiger, B., Vienneau, D., de Hoogh, K., Röösli, M., Ragettli, M.S., 2024. Socio-environmental modifiers of heat-related mortality in eight Swiss cities: A case time series analysis. *Environ. Res.* 246.
- Yang, J., Ou, C.-Q., Ding, Y., Zhou, Y.-X., Chen, P.-Y., 2012. Daily temperature and mortality: a study of distributed lag non-linear effect and effect modification in Guangzhou. *Environ. Health* 11, 1–9.
- Yang, J., Zhou, M., Ren, Z., Li, M., Wang, B., Liu, L., Ou, C.Q., Yin, P., Sun, J., Tong, S., Wang, H., Zhang, C., Wang, J., Guo, Y., Liu, Q., 2021. Projecting heat-related excess mortality under climate change scenarios in China. *Nat. Commun.* 12, 1039.
- Yao, R., Wang, L., Huang, X., Niu, Y., Chen, Y., Niu, Z., 2018. The influence of different data and method on estimating the surface urban heat island intensity. *Ecol. Ind.* 89, 45–55.
- Zhang, K., Cao, C., Chu, H., Zhao, L., Zhao, J., Lee, X., 2023. Increased heat risk in wet climate induced by urban humid heat. *Nature* 617, 738–742.
- Zhang, X., Friedl, M.A., Schaaf, C.B., Strahler, A.H., Schneider, A., 2004. The footprint of urban climates on vegetation phenology. *Geophys. Res. Lett.* 31, n/a-n/a.
- Zhao, Q., Guo, Y., Ye, T., Gasparrini, A., Tong, S., Overcenco, A., Urbán, A., Schneider, A., Entezari, A., Vicedo-Cabrera, A.M., Zanobetti, A., Analitis, A., Zeka, A., Tobias, A., Nunes, B., Ahmad, B., Armstrong, B., Forsberg, B., Pan, S.C., Iniguez, C., Ameling, C., De la Cruz Valencia, C., Astrom, C., Houthuijs, D., Dung, D.V., Roye, D., Indermitte, E., Lavigne, E., Mayvaneh, F., Acquaotta, F., de' Donato, F., Di Ruscio, F., Sera, F., Carrasco-Escobar, G., Kan, H., Orru, H., Kim, H., Holobaca, I.H., Kysely, J., Madureira, J., Schwartz, J., Jaakkola, J.J.K., Katsouyanni, K., Hurtado Diaz, M., Ragettli, M.S., Hashizume, M., Pascal, M., de Sousa Zanotti Staglario Coelho, M., Valdes Ortega, N., Ryti, N., Scovronick, N., Michelozzi, P., Matus Correa, P., Goodman, P., Nascimento Saldiva, P.H., Abrutzky, R., Osorio, S., Rao, S., Fratianni, S., Dang, T.N., Colistro, V., Huber, V., Lee, W., Seposo, X., Honda, Y., Guo, Y.L., Bell, M.L., & Li, S. (2021). Global, regional, and national burden of mortality associated

- with non-optimal ambient temperatures from 2000 to 2019: a three-stage modelling study. *Lancet Planet Health*, 5, e415-e425.
- Zhao, L., Lee, X., Smith, R.B., Oleson, K., 2014. Strong contributions of local background climate to urban heat islands. *Nature* 511, 216–219.
- Zhou, B., Rybski, D., Kropp, J.P., 2013. On the statistics of urban heat island intensity. *Geophys. Res. Lett.* 40, 5486–5491.
- Zhou, B., Lauwaet, D., Hooyberghs, H., De Ridder, K., Kropp, J.P., Rybski, D., 2016. Assessing Seasonality in the Surface Urban Heat Island of London. *J. Appl. Meteorol. Climatol.* 55, 493–505.
- Zhou, B., Rybski, D., Krop, J.P., 2017. The role of city size and urban form in the surface urban heat island. *Sci Rep* 7, 4791.
- Zhou, D., Sun, S., Li, Y., Zhang, L., Huang, L., 2023. A multi-perspective study of atmospheric urban heat island effect in China based on national meteorological observations: Facts and uncertainties. *Sci. Total Environ.* 854, 158638.
- Zhu, W., Yuan, C., 2023. Urban heat health risk assessment in Singapore to support resilient urban design—By integrating urban heat and the distribution of the elderly population. *Cities* 132, 104103.
- Zhu, D., Zhou, Q., Liu, M., Bi, J., 2021. Non-optimum temperature-related mortality burden in China: Addressing the dual influences of climate change and urban heat islands. *Sci. Total Environ.* 782, 146760.